A Frequency Diversity Algorithm for Extending the Radar Doppler Velocity Nyquist Interval

V. Venkatesh*, L. Li†, M. McLinden†, M. Coon†, G. M. Heymsfield†
* Jet Propulsion Lab † NASA/Goddard Space Flight Center

Abstract

Compact millimeter wavelength radars have been widely used for applications such as remote sensing of clouds, guidance avionics and recently, automotive navigation. However, the short wavelength of these radars limit their maximum unambiguous Doppler velocity. A common solution to this problem is to subsequently unfold the Doppler velocity estimate with the staggered pulse repetition time (PRT) algorithm, which requires two different PRTs to be employed in sequence. This work investigates a novel and potentially more rapid method to extend the Doppler velocity Nyquist interval. The investigated algorithm uses a pair of frequency diverse pulses separated by a short time lag for Doppler velocity estimation while the unambiguous range still corresponds to the pulse repetition time employed. During the first PRT, two pulses with center frequencies f_1 followed by f_2 separated by a lag τ are transmitted. During the next PRT, the pulses transmitted are in the order f_2 followed by f_1. Doppler velocity is then estimated using the sum of the Doppler phases derived from f_1/f_2 and f_2/f_1 sequences. Based on Monte-Carlo simulations and data collected with the NASA Goddard Space Flight center (GSFC) Cloud Radar System (CRS), the algorithm is demonstrated on surface echoes. Projected aircraft speeds and traditional pulse-pair estimates were employed as a reference. The novel algorithm was found to perform adequately for a low spectrum width of the order of 0.5 m/s and SNR better than 20 dB. A simple-point target based model is used to interpret results, and simulations are used as a baseline to transition from point-target to surface scattering scenarios.

Index Terms

Corresponding author email : vijay.venkatesh@jpl.nasa.gov .

Millimeter wave radar, algorithm design, data analysis, signal processing, Doppler velocity. Frequency diversity, pulse-pair.

I. INTRODUCTION

Millimeter wave radars have been used for applications such as atmospheric remote sensing [1], [2], [3], target tracking [4], [5], guidance and navigation [6], [7]. In part, the popularity of these millimeter wave radars is because short wavelengths (λ) allow fine angular resolution to be realized while still allowing for physically small and lightweight designs. The choice of a short wavelength however exacerbates the range-Doppler ambiguity dilemma in pulse trains. For a given pulse repetition time (T), the unambiguous Doppler velocity (v_u) is given by $v_u = \frac{\lambda}{4T}$ while the unambiguous range (R_u) is given by $R_u = \frac{cT}{2}$. Since pulse repetition time is directly proportional to R_u but inversely proportional to v_u, a "see-saw" trade results. This trade is exacerbated at short wavelengths, since v_u is proportional to λ. Millimeter wavelength radars that are required to have long range coverage often have Doppler Nyquist intervals that are much smaller than the relative speeds of target with respect to the platform.

Techniques to mitigate the Doppler-Range ambiguity dilemma have been developed. For example, the staggered PRT [8] and Polarization Diversity Pulse-Pair (PDPP) [9] techniques decouple the maximum unambiguous range from the maximum unambiguous Doppler velocity. The staggered PRT is a multi-rate sampling method that unfolds the Doppler velocity based on differential aliasing in Doppler velocities measured using 2 unique Pulse Repetition Times (PRT). The idea is that as the true velocity increases, it aliases onto different values within the two Doppler Nyquist intervals. Depending on the difference in measured Doppler velocities from the 2 PRTs, a correction is computed. A limitation of the staggered PRT method is that the dwell time approaches double that of single PRT operation. This is because of the need to estimate Doppler velocity with sufficient precision sequentially at two lags. The Polarization Diversity Pulse-Pair method provides more rapid measurements than staggered PRTs by using a significantly shorter lag τ between the pulses used for Doppler velocity estimation and eliminating the need for a dwell with a second PRT. Here, two pulses with orthogonal polarizations are placed within a PRT and Doppler velocity is estimated by cross-correlating voltages from these two pulses with orthogonal polarizations. The unambiguous Doppler velocity now corresponds to the lag between the pair of pulses with orthogonal polarizations, while the unambiguous range still corresponds to the PRT. For non-depolarizing scatterers, the cross-polarization isolation of the antenna provides a mechanism to isolate returns from each polarization. A limitation of this method is the need for additional microwave hardware such as an orthomode transducer and dual-polarized feeds for the antenna. Spillage due to finite cross-polarization isolation may further limit the extent of Doppler retrievals within profiles that have high SNR regions [10]. This is often the case for downward looking radars because the surface echo is atleast one high SNR region with a profile.

This work investigates a novel approach that uses frequency diverse waveforms for Doppler velocity estimation [11]-[12]. Relative to the polarization diversity, isolation is traded for coherence. For applications where this loss in coherence is not precipitous, digital filters provide isolation that is several orders of magnitude better than antenna cross-polarization isolation at millimeter wavelengths. Similar methods have been formulated for use in automotive radars [13], and the novel part herein is the adaptation and subsequent demonstration to a beam-filled scenario with non-trivial spectrum width. Numerical simulations and analysis of real data are used to demonstrate this novel algorithm. The following section outlines a conceptual formulation of the Frequency Diversity Pulse-Pair algorithm (FDPP) using a point-target model. Subsequently, numerical simulations are employed as a baseline to transition from point-target to surface scattering scenarios. Finally, surface echo data is used to demonstrate the algorithm using projected aircraft speeds and traditional pulse-pair measurements as references.

II. ALGORITHM FORMULATION

The algorithm proposed herein decouples unambiguous velocity from unambiguous range by employing two frequency shifted waveforms within a pulse repetition period. As shown in Fig. 1, the two transmitted pulses at center frequencies of f_1 and f_2 are separated by a time-lag τ. The order of transmitted frequencies is reversed after every transmit/receive cycle while retaining the same lag τ. The choice of f_1 and f_2 is such that the return signals can be separated by filters implemented in the digital receiver. Cross-covariances from the two sequences are individually accumulated and stored (denote as as c_{12} and c_{21} respectively). Doppler velocity is then estimated from the sum of the cross-covariance estimates from each pair.

Herein, a simple point target based analysis of the phase estimate produced by the FDPP algorithm is presented. A more detailed analytical treatise may be found in [11], and we present a simplified model herein. Denote the received voltage at the antenna at frequency f_1 due to a

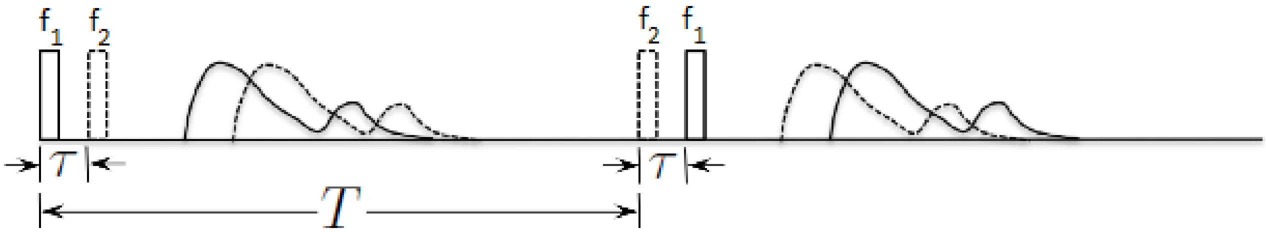

Fig. 1: Illustration of the Frequency Diverse Pulse-Pair (FDPP) algorithm concept. The first sequence transmitted has two frequencies f_1 followed by f_2 and separated by lag τ. After one elapsed pulse-repetition time T, the next transmitted sequence has f_2 followed by f_1 separated by the same lag τ. The concept is that errors and range dependent phase terms between the f_1/f_2 and f_2/f_1 pairs cancel out.

point-target at range R as [14]

$$V_1(t) = S_1 exp\{-2jk_1R\}. \tag{1}$$

For the same range-bin of interest, the received voltage at frequency 2 after a time-lag τ, can be written as

$$V_2(t+\tau) = S_2 exp\{-2jk_2(R + v_r\tau)\}, \tag{2}$$

where v_r is the radial velocity of the scatterer towards or away from the radar, S_1 and S_2 are radar system dependent constants. Since this component of velocity causes the most phase shifts, it suffices to consider this component of scatterer motion alone. Assuming the random process to be wide-sense stationary, we may omit the dependence on t and express the covariance of the f_1/f_2 pair as

$$\langle c_{12}(\tau)\rangle = \langle V_1^* V_2(\tau)\rangle \approx S_1S_2 exp\{-[2j(k_2 - k_1)R + (2k_2v_r\tau)]\}, \tag{3}$$

During the next pulse repetition interval, the covariance of the f_2/f_1 pair is

$$\langle c_{21}(\tau)\rangle = \langle V_2^* V_1(\tau)\rangle \approx S_1S_2 exp\{-[2j(k_1 - k_2)R + (2k_1v_r\tau)]\}. \tag{4}$$

Now denote the phase of the covariances as

$$\langle \Delta\phi_{12}\rangle = \angle\langle c_{12}(\tau)\rangle, \tag{5}$$

$$\langle \Delta\phi_{21}\rangle = \angle\langle c_{21}(\tau)\rangle. \tag{6}$$

The sum of the phases of the two covariances can be written as

$$\langle \Delta\Phi \rangle = \langle \Delta\phi_{12} \rangle + \langle \Delta\phi_{21} \rangle. \tag{7}$$

Using (3) and (4) in (7), the phase of the covariance sum simplifies as

$$\langle \Delta\Phi \rangle = 2(k_1 + k_2)\tau \; v_r. \tag{8}$$

The implementation we consider herein typically has frequencies that are separated by several MHz for a millimeter wave radar, such as a 94 GHz W-band radar system. Therefore, we approximate $k_1 + k_2 \approx 2k_1$. The above equation simplifies to

$$v_r = \frac{1}{4k_1\tau}\langle \Delta\Phi \rangle. \tag{9}$$

Since all values other than $\Delta\Phi$ are solely system dependent, the radial component of target mean radial velocity v_r can be obtained from the ensemble-averaged $\Delta\Phi$. Two comments about the Nyquist velocity of the frequency diversity pulse-pair estimates are in order. First, for a given lag τ the Nyquist interval is diminished by a factor of 2 compared to a traditional pulse-pair or a polarization diversity pulse-pair. This is because the frequency diversity pulse-pair algorithm accumulates two phase estimates $\Delta\phi_{12}$ and $\Delta\phi_{21}$ and each of these variables that form the resultant sum have a range of variation from $[-\pi, \pi]$. This is in contrast to the traditional pulse-pair algorithm which directly uses a phase estimate ranging from $[-\pi, \pi]$. Second, the frequency diversity pulse-pair algorithm developed herein allows an extension of the Nyquist interval as compared to a traditional pulse-pair which necessarily needs long lags to accommodate sufficiently large unambiguous ranges. For example, if the FDPP estimate is obtained with a lag τ and the traditional pulse-pair estimate is obtained with a lag T, then the Nyquist interval of the FDPP algorithm is improved by a factor $\frac{T}{2\tau}$.

A brief analysis of the variance of $\Delta\Phi$ reveals a mechanism that partially alleviates the loss of pulse-pair coherence due to Rayleigh fading. Let Var denote the variance operator, Cov denote the covariance operator and ρ denote the correlation operator for the random variables $\Delta\Phi_{12}$ and $\Delta\Phi_{21}$. From (7), we know that

$$Var(\Delta\Phi) = Var(\Delta\Phi_{12}) + Var(\Delta\Phi_{21}). + 2Cov(\Delta\Phi_{12}, \Delta\Phi_{21}) \tag{10}$$

Now, the covariance term can be conveniently decomposed as

$$Cov(\Delta\Phi_{12}, \Delta\Phi_{21}) = \rho(\Delta\Phi_{12}, \Delta\Phi_{21}) \cdot \sqrt{Var(\Delta\Phi_{12}) \cdot Var(\Delta\Phi_{21})} \tag{11}$$

Since the same time-lag τ is used for the f_1/f_2 pair and the f_2/f_1 pair, $Var(\Delta\Phi_{12}) = Var(\Delta\Phi_{21})$,

$$Cov(\Delta\Phi_{12}, \Delta\Phi_{21}) = \rho(\Delta\Phi_{12}, \Delta\Phi_{21}) \cdot Var(\Delta\Phi_{12}) \tag{12}$$

From the above relationships,

$$Var(\Delta\Phi) = 2Var(\Delta\Phi_{12}) + 2\rho(\Delta\Phi_{12}, \Delta\Phi_{21}) \cdot \sigma(\Delta\Phi_{12}) \tag{13}$$

Rearranging terms in (13),

$$Var(\Delta\Phi) = 2Var(\Delta\Phi_{12})[1 + \rho(\Delta\Phi_{12}, \Delta\Phi_{21})] \tag{14}$$

From (14), we see that as $\rho(\Delta\Phi_{12}, \Delta\Phi_{21})$ tends to -1, $Var(\Delta\Phi)$ tends to 0. In other words, the variances of the f_1/f_2 and f_2/f_1 phase estimates can be large since there is little correlation between the f_1 and f_2 pulses. However, if the f_1/f_2 and f_2/f_1 phase estimates are highly anti-correlated, the sum of the two phase estimates has a much smaller variance. For sufficiently small Doppler velocities in (3) and (4), it can be shown than $\rho(\Delta\Phi_{12}, \Delta\Phi_{21}) = -\rho(\Delta\Phi_{12}, \Delta\Phi_{12})$. For low velocity turbulence and short lags, it appears reasonable to approximate the auto-correlation $\rho(\Delta\Phi_{12}) \approx 1$. This is turn results in $\rho(\Delta\Phi_{12}, \Delta\Phi_{21}) \approx -1$.

Note that a similar identity was first exploited on contiguous pulse-pairs [15]. The difference here is that alternating f_1/f_2 and f_2/f_1 pairs brings about an anti-correlation, as opposed to the "common pulse" in contiguous pulse-pairs. The algorithm herein has more similarities to the alternating polarization sequence used for "Differential propagation phase shift" (Φ_{DP}) measurements in [16]. In that case, it was shown that the correlation between phase estimates from an alternately reversing sequence approaches -1 for zero spectrum width and $SNR > 20$ dB (equation 6.57 in [17]).

III. PERFORMANCE EVALUATION

A. Simulations

The point-target based model in the earlier section was solely meant to aid interpretation. Numerical simulations are used as a baseline to go from point-target to beam-filled scattering. The approach to simulations adopted herein is to compute backscattered voltages using a Monte-Carlo like simulator [18] and estimate the phases at lag τ on the simulated voltages. The voltage at the radar receiver due to a collection of scatterers is given as

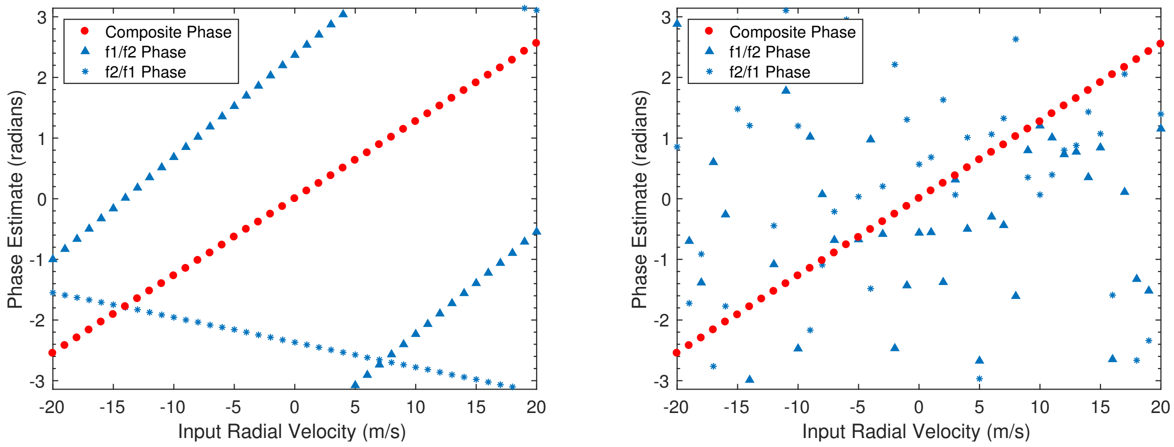

(a) Spectrum Width = 0 m/s
Number of Scatterers = 1

(b) Spectrum Width = 0 m/s
Number of Scatterers = 1000

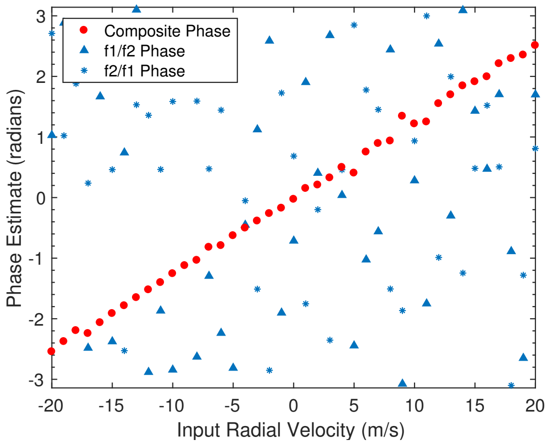

(c) Spectrum Width = 1 m/s
Number of Scatterers = 1000

Fig. 2: Monte-Carlo simulations showing the frequency diversity Doppler estimation algorithm concept. As the number of scatterers increase, the f1/f2 and f2/f1 pair phases become increasingly “noisy”. Nonetheless, the composite phase (sum of f1/f2 and f2/f1 phase) produces a good estimate of Doppler velocity for trivial spectrum width.

$$V(t) = W \sum_{n=1}^{N_s} A_n R_n \exp\{-2jkr_n\}. \tag{15}$$

Here, W is the radar constant for beam-filled surface scattering. Further, n denotes the n^{th} scatterer, A_n denotes the antenna weighting function and R_n denotes the range weighting function evaluated for the n^{th} scatterer. The antenna weighting function is defined below

$$A(X_n, Y_n) = \exp\left\{-\frac{(X_0 - X_n)^2}{2r_0^2\sigma_\phi^2} - \frac{(Y_0 - Y_n)^2}{2r_0^2\sigma_\theta^2}\right\} \tag{16}$$

where the antenna phase center is denoted by $[X_0, Y_0]$ and is the origin for the co-ordinate system adopted herein. The scatterer locations are indicated by $[X_n, Y_n]$ and σ_ϕ and σ_θ are the second central moments of the effective two way antenna patterns in the azimuthal and elevation planes respectively. These are related to antenna 3-dB beamwidths by the relationship

$$\sigma_\phi = \frac{\theta_{3dB}}{\sqrt{(8 * ln2)}} \tag{17}$$

where, θ_{3dB} denotes the antenna 3 dB beamwidth. The range weighting function is given by

$$R(Z_n) = \exp\left\{-\frac{(Z_0 - Z_n)^2}{2\sigma_R^2}\right\} \tag{18}$$

where, Z_0 is the range to the center of the resolution volume and Z_n indicates the scatterer location [18]. The location of each scatterer is updated at every pulse repetition interval τ using the relationship $\vec{P_n} = \vec{P_n} + \vec{v_n}\tau$. Here, $\vec{P_n}$ denotes the three-dimensional position of the scatterer and $\vec{v_n}$ denotes the velocity of each scatterer. Each component of three-dimensional velocity is in turn decomposed into deterministic and random velocity components. Gaussian distributed zero-mean random variables are used to synthesize the turbulent velocity fields. As the scatterers evolve, the voltages at the frequencies of interest are obtained in a manner consistent with Fig. 1. After scaling to the desired SNR, thermal noise is added to the synthesized signals at the respective frequencies before the phase estimates are produced, after scaling for the desired SNR. Phase estimates at the lag τ are then obtained for the sequences f_1/f_2 and f_2/f_1. These phase estimates are then added and subsequently scaled using equation (9) to obtain Doppler velocity.

Fig. 2 shows simulated estimates of Doppler velocity using the frequency diverse algorithm for a dwell time of 100 ms. Here, “composite phase” is the sum of the f_1/f_2 and f_2/f_1 phases after wrapping into the interval [$-\pi$,π]. As is evident in Fig. 2a and Fig. 2c, the algorithm works well for a point scatterer. As the number of scatterers alone is increased, the estimator still holds up well. But the combination of Rayleigh fading and spectrum width degrades the precision of the Doppler estimate. Consequently, the application of the algorithm is limited to beam-filled scenarios with low spectrum width.

B. Data analysis

To evaluate performance, the FDPP technique was implemented on the NASA Goddard Space Flight Center (GSFC) W-band Cloud Radar System (CRS) during the 2015 NASA Olympic Mountain Experiment (OLYMPEX) and the 2017 NOAA Geostationary Operational Environmental Satellite R (GOES-R) series calibration campaign. During these field campaigns, CRS was installed on the NASA ER-2 aircraft along with the other sensors for cloud and precipitation observation. Fig. 3 shows qualitative comparisons of FDPP retrievals on isolated surface echoes with traditional pulse-pair measurements. Simulations are used as a baseline to interpret differences between traditional pulse-pair and FDPP Doppler estimates. CRS was mounted on an ER-2 aircraft with the antenna pointed near nadir. Pointing angle deviations away from nadir are introduced because of antenna mounting errors and aircraft attitude. In turn, this induces a non-zero surface velocity measurement due the motion of the aircraft. In Fig. 3, "Measured pulse-pair velocities" shown in Fig. 3a and the error sources shown in Fig. 3b were used as inputs to the simulation. The simulation output is shown by the red dotted line in Fig. 3a and aids interpretation of the FDPP algorithm performance. Two comments are in order. First, FDPP estimates of Doppler velocity are in reasonable agreement with traditional pulse-pair Doppler velocity estimates in regions of high SNR (i.e. of the order of 20 dB). This constitutes a qualitative demonstration of the algorithm concept developed herein. Second, both FDPP measurements from CRS and simulations show large deviations from the pulse-pair Doppler velocity estimate in regions of low SNR (i.e. comparable to 0 dB). This is because the error cancellation mechanism of the FDPP algorithm relies on high anti-correlation between the f_1/f_2 pair and the f_2/f_1 pair. Recall that thermal noise is merely uncorrelated.

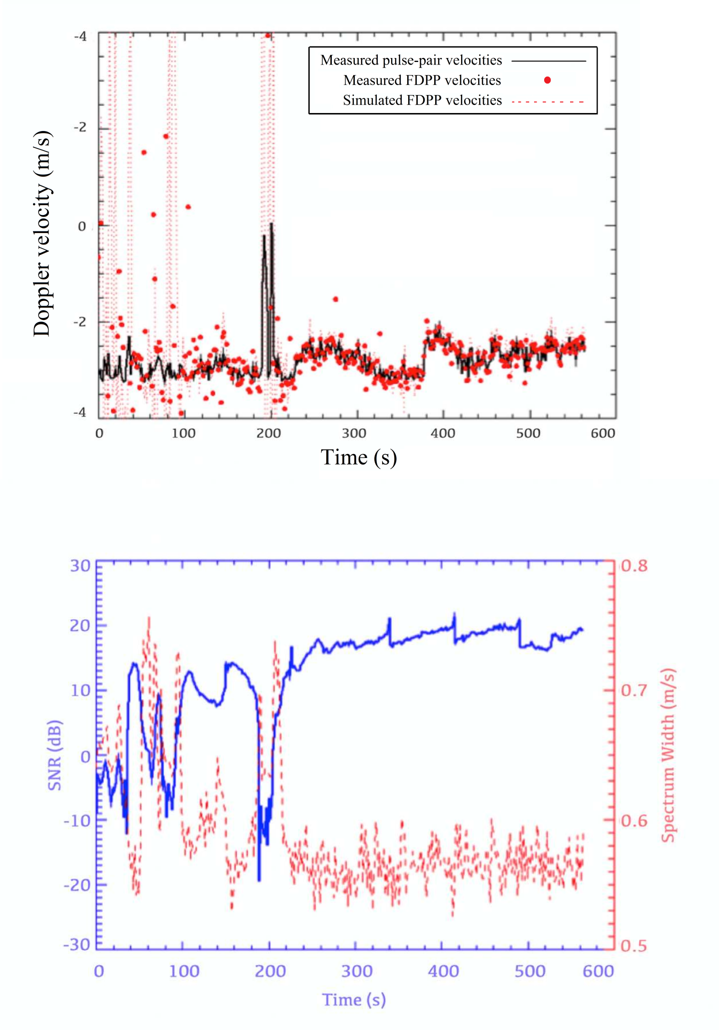

Fig. 3: Top - Evaluation of frequency diversity Doppler velocity measurements using traditional pulse-pair measurements as a reference. Simulations are employed as a baseline for interpretation. While the FDPP algorithm performs well for SNR of the order of 20 dB, both measurements and simulations show that the algorithm has poor immunity to thermal noise. Bottom - SNR and spectrum width corresponding to the duration over which the measurements were made. The "blue" line corresponds to SNR in dB and the "red" line corresponds to Spectrum width in m/s.

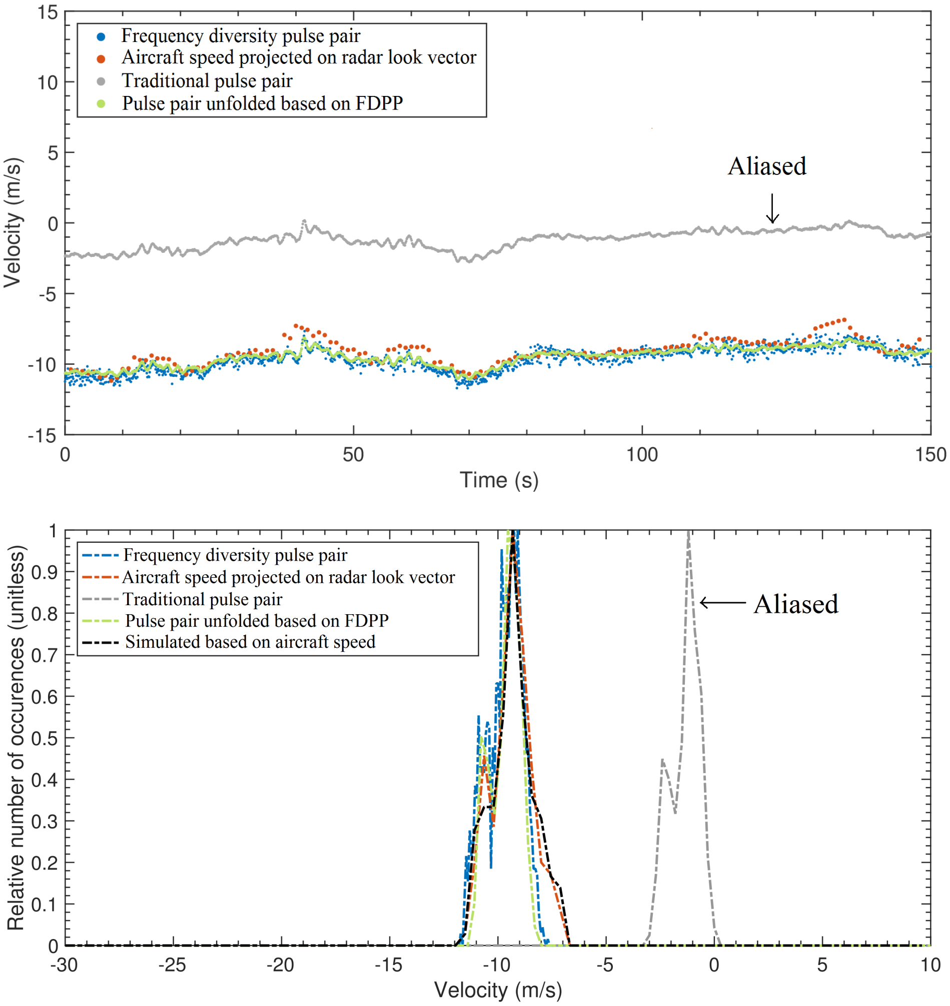

Fig. 4: Comparison of FDPP and pulse-pair measurements of Doppler velocity using projected aircraft speed as a reference. Top - While traditional pulse-pair estimates are aliased, FDPP estimates of Doppler velocity agree with aircraft speed projections on the radar look vector. However, unfolded pulse-pair velocities using the pulse-pair as reference show that the FDPP has a higher standard deviation relative to the traditional pulse-pair estimator. Bottom - The probability density functions of simulated FDPP Doppler estimates are in qualitative agreement with measurements. The simulations herein used projected aircraft speeds as input.

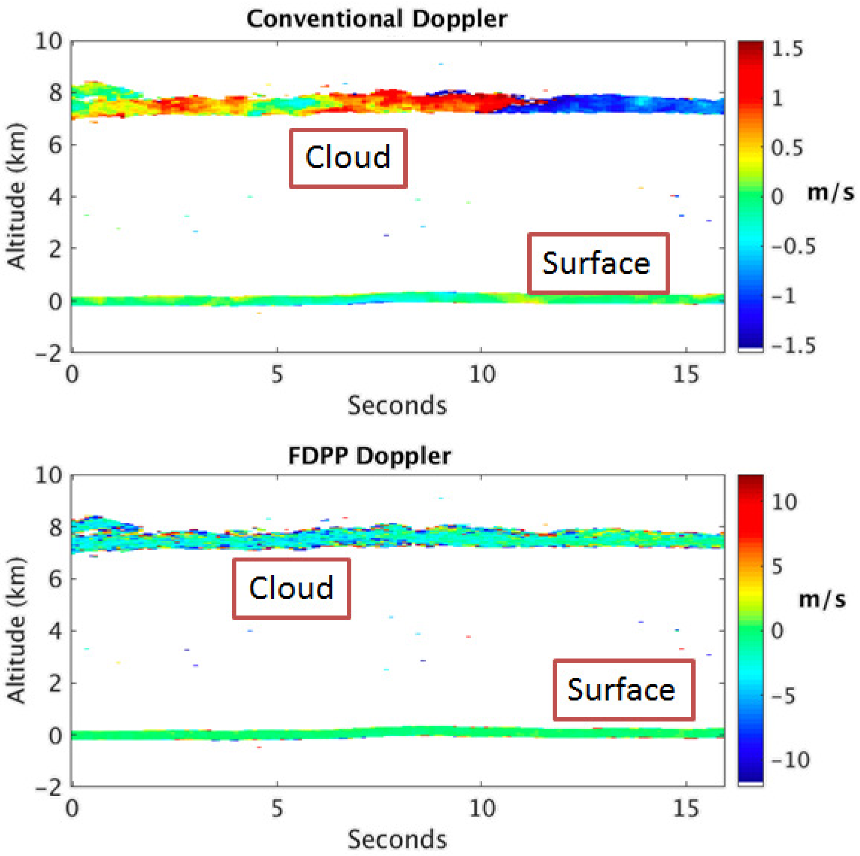

Fig. 5: Cloud radar System (CRS) Doppler velocity measurements from the NOAA GOES-R validation campaign. The dataset was collected on May 17th, 2017 at 03:53 UTC with the antenna was pointing “nearly” at nadir. Top - Traditional pulse-pair measurements in clouds show significant folding over the flight segment. Bottom - Frequency Diverse Pulse-pair measurements (FDPP) in clouds show little folding over the same flight segment. Surface Doppler measurements show little folding in both cases and are better suited for subsequent quantitative comparisons.

During one of the GOES-R flights, the ER-2 aircraft pilot performed high pitch maneuvers. For one of these high pitched measurements, Fig. 4 shows FDPP measurements of Doppler velocity compared to conventional pulse-pair velocities using projected aircraft speed as a reference. The aircraft attitude was recorded using an Inertial Motion Unit and measured velocity, roll, pitch, and heading. The geometric projection of the aircraft motion vector onto the radar look vector gives the radial velocity that is employed as a reference herein. To compute this projection, two coordinate system are defined; track relative and aircraft relative. The track relative coordinate system is assumed to be static and representative of aircraft motion. The aircraft relative coordinate system express the orientation of the aircraft for a given roll, pitch, and drift. The rotation of the aircraft relative coordinate system can be mapped to track relative coordinate system using 3 rotation matrices [19]

$$M_P = \begin{bmatrix} 1 & 0 & 0 \\ 0 & cos(P) & -sin(P) \\ 0 & sin(P) & -cos(P) \end{bmatrix},$$

$$M_D = \begin{bmatrix} cos(D) & -sin(D) & 0 \\ sin(D) & cos(D) & 0 \\ 0 & 0 & 1 \end{bmatrix}, \tag{19}$$

$$M_R = \begin{bmatrix} cos(R) & 0 & sin(R) \\ 0 & 1 & 0 \\ -sin(R) & 0 & cos(R) \end{bmatrix}.$$

The initial look vector of the antenna is given by

$$X_a = \begin{bmatrix} x_a \\ y_a \\ z_a \end{bmatrix} = \begin{bmatrix} cos(\tau_a)sin(\theta_a) \\ sin(\tau_a) \\ cos(\theta_a)cos(\tau_a) \end{bmatrix}. \tag{20}$$

The off-nadir pitch offset of 2.8 degrees in Fig. 4 corresponds to $\theta_a = \pi$ and$\tau_a = 2\pi - 2.8^o$ in equation (21). Finally, the rotation order is given by:

$$X_t = M_d M_P M_R X_a \tag{21}$$

where X_t is the track relative coordinate and X_a is the aircraft relative coordinate system. Finally, the dot-product of X_t with the Cartesian aircraft motion vector gives the projected radial velocity. Using the projected radial velocity as a reference, we note that the FDPP measurements of Doppler velocity are in qualitative agreement in the expected value sense, while traditional pulse pair velocities are aliased. The pulse-pair velocities shown herein correspond to a pulse repetition time of 247 micro-seconds. However, the conventional pulse-pair measurements have a lower standard deviation than the FDPP estimates of Doppler velocity. This is because of the inevitable loss of coherence due to frequency swinging. Since pulse-pair estimates are already available in the time-series, we find that the best estimator of Doppler velocity is to use the FDPP as a reference to unfold traditional pulse-pair estimates. In this manner, the higher Doppler Nyquist interval of the FDPP for sufficiently high SNR may be combined with the lower standard deviation of the pulse-pair estimates. Lastly, the simulated statistics using the aircraft speed projections as input are in qualitative agreement with measurements for dwell times of 0.5 seconds. This validates the simulation methodology and the deductions made therein.

Fig. 5 shows Doppler velocity estimates made with the traditional pulse-pair algorithm and the frequency diverse method investigated herein. Here, the surface is at an altitude that is nearly 0 km while a thin layer of cirrus cloud is at an altitude of approximately 7.5 km. We see that there is little folding in the FDPP and traditional pulse-pair measurements from surface echoes with little motion along the radial direction. But the upward motion of the cirrus cloud makes traditional pulse-pair estimates of Doppler velocity fold more than the FDPP Doppler estimate. Here, traditional pulse-pair Doppler velocity estimates were made with a PRT of 504 microseconds. We also note that the FDPP algorithm yields noisier estimates on clouds as compared to a nearly static surface. This can be attributed to the loss in coherence in clouds relative to surface echoes. For the dataset shown here, the mean coherence in the surface echoes was 0.92 while the mean coherence in the cloud layer was 0.06. The reason we get some coherent Doppler velocity structure in the clouds is because significant phase anti-correlation brings about a cancellation of the variances of the f_1/f_2 and the f_2/f_1 pairs. Notwithstanding, we see that there is significantly less folding in the FDPP Doppler estimate in the cloud layer compared to traditional pulse-pair Doppler measurements. This shows that the frequency diversity algorithm investigated herein has a wider Nyquist interval for the Doppler velocity estimate relative to traditional pulse-pair measurements. However, it appears based on data that the FDPP Doppler estimates from surface echoes have significantly better precision than Doppler retrievals in clouds. This may potentially be attributed to differences in scattering mechanisms and are not well understood at this juncture. Further study is necessary in order to benchmark and potentially optimize the performance of the FDPP algorithm across there scattering mechanisms.

IV. SUMMARY

Waveforms with frequency diversity have been employed for mitigating the range-Doppler ambiguity dilemma in automotive radars [13]. The novel part in this work was the random phase error and range dependent term self-cancelling algorithm design and the demonstration in a beam-filled scenario. With modern waveform generation, digital receiver and solid-state power amplifier technologies, the frequency diversity algorithm can be implemented without additional hardware such as a second millimeter wave receive chain. The transmit waveform sequence was muliplexed in time through the transmitter and already available electronics in the radar system. On receive, digital filters isolated returns from each of the frequencies. During the first PRT, the radar system transmitted a sequence of two pulses modulated by frequencies f_1 and f_2 in that order. During the next PRT, the order of f_2 and f_1 were reversed. The sum of the phase estimates from the f_1/f_2 and f_2/f_1 pairs yielded a composite phase which is linearly proportional to Doppler velocity.

The algorithm concept was investigated using Monte-Carlo simulations and data collected with the NASA GSFC's Cloud Radar System. A simple point-target based analytical formulation enabled interpretation of results. Simulations were employed to go between point-target and surface scattering. On data collected with the NASA Cloud Radar System, the surface echo Doppler estimates made with the FDPP algorithm were in reasonable agreement with traditional pulse-pair velocites for a low antenna pitch offset. On a flight where aircraft maneuvers were performed to result in high antenna pitch angles, the pulse-pair Doppler velocities from the surface were aliased while the FDPP Doppler estimate was in agreement with projected aircraft speed. The algorithm was found to perform well for a spectrum width of about 0.5 m/s and SNR greater than 20 dB. There were two mechanisms for error reduction. First, the phases due to the difference frequency from the f_1/f_2 and f_2/f_1 pairs canceled out in the expected value sense. Second, the sum of the two phase estimates has a much smaller variance relative to the individual phase estimates since the f_1/f_2 and f_2/f_1 phase estimates are highly anti-correlated.

FDPP Doppler estimates in clouds were found to have lower precision than surface echoes. However, the lack of sufficient SNR in clouds made it difficult to attribute differences in precision due to the scattering mechanism alone. Future work may focus on using the frequency diverse pulse-pair as a reference to optimally unfold Doppler estimates from a single PRT. In addition to being used for correcting air-borne antenna pointing errors using the surface echo, this FDPP algorithm may also be investigated for use in terminal descent sensors that provide spacecraft guidance and navigation signals [20].

ACKNOWLEDGMENT

This work was supported under the NASA Instrument Incubator Program award NNH13ZDA001N. At the time of completing the work, Vijay Venkatesh was supported by the JPL Research and Technology Development Award 01SCTR/R.18.021.070 .

REFERENCES

[1] R. Tanamachi, H. Bluestein, W. Lee, M. Bell, and A. Pazmany, “Ground-based velocity track display (gbvtd) analysis of w-band doppler radar data in a tornado near stockton, kansas on 15th may 1999,” *Mon. Wea. Rev.*, pp. 783–800, 2007.

[2] L.Li, G. Heymsfield, P. Racette, L. Tian, and E. Zenker, “A 94 ghz cloud radar system on a nasa high-altitude er-2 aircraft,” *J. Atmos. Oceanic. Tech.*, pp. 1378–1388, 2004.

[3] G. Stephens, “The cloudsat mission and the a-train : A new dimension of space-based observations of clouds and precipitation,” *Bull. Amer. Meteor. Soc.*, vol. 83, pp. 1771–1790, 2002.

[4] J. Stambaugh and R. Lee, “The 4 ghz bandwidth millimeter wave radar,” *Lincoln Laboratory Journal*, pp. 64–76, 2012.

[5] S. Patole, M. Torlak, D. Wang, and M. Ali, “Automotive radars : A review of signal processing techniques,” *IEEE Sig. Pro. Mag.*, pp. 22–35, 2017.

[6] G. Brooker, D. Birch, and J. Solms, “W-band airborne interrupted frequency modulated cw imaging radar,” *IEEE Trans. Aerosp. Electron. Syst.*, pp. 995–972, 2005.

[7] F. Sajadi, M. Helgeson, M. Radke, and G. Steyn, “Radar synthetic vision system for adverse weather aircraft landing,” *IEEE Trans. Aerosp. Electron. Syst.*, pp. 2–14, 1999.

[8] M. Sachidananda and D. Zrnic, “Unambiguous range extension by overlay resolution in staggered prt technique,” *J. Atmos. Oceanic. Tech.*, pp. 673–684, 2003.

[9] A. Pazmany, J. C. Galloway, J. Mead, I. Popstefanija, R. McIntosh, and H. Bluestein, “Polarization diversity pulse-pair technique for millimeter wave doppler radar measurements of severe storm measurements,” *J. Atmos. Oceanic. Tech.*, pp. 1900–1911, 1999.

[10] A. Battaglia and S. Tanelli, “Polarization diversity for millimeter wave spaceborne doppler radars: An answer for observing deep convection ?” *J. Atmos. Oceanic. Tech.*, vol. 30, pp. 2768–2787, 2013.

[11] L. Li, M. McLinden, M. Coon, G. Heymsfield, and V. Venkatesh, “Frequency diversity pulse pair determination for mitigation of range-doppler ambiguity,” *US patent*, Issued Dec. 21, 2017.

[12] G. Heymsfield and L. Miller, “Method for ambiguity resolution in range-doppler measurements,” *US patent 5*, Issued Dec. 28, 1995.

[13] M. Kronauge and H. Rohling, “New chirp sequence radar waveform,” *IEEE Trans. Aerosp. Electron. Syst.*, pp. 2870–2877, 2014.

[14] R. J. Doviak, R. J. Lataitis, and C. L. Holloway, “Cross correlations and cross spectra for spaced antenna wind profilers part i: Theoretical analysis,” *Radio Sci.*, vol. 31, pp. 157–180, 1996.

[15] D. Zrnic, “Spectral moment estimates from contiguos pulse-pairs,” *IEEE Trans. Aerosp. Electron. Syst.*, pp. 344–354, 1977.

[16] M. Sachidananda and D. Zrnic, “Differential propagation phase shift and rainfall rate estimation,” *Radio Sci.*, vol. 21, no. 2.

[17] R. J. Doviak and D. S. Zrnić, *Doppler Radar and Weather Observations, 2nd ed.* Academic Press, 1993.

[18] V. Venkatesh and S. J. Frasier, “Simulation of spaced antenna wind retrieval performance on an x-band active phased-array weather radar,” *J. Atmos. Oceanic. Tech.*, pp. 1447–1459, 2013.

[19] W. Lee, P. Dodge, F. Marks, and P. Hildebrand, “Mapping of airborne doppler radar data,” *J. Atmos. Oceanic. Tech.*, vol. 11, pp. 572–578, 1994.

[20] J. Eichler, “A performance study of the lunar module’s landing radar system,” *J. Spacecraft*, pp. 1016–1022, 1968.